*hydrology*

MDPI

*Article*

# Soil–Water–Atmosphere Effects on Soil Crack Characteristics under Field Conditions in a Semiarid Climate

**Jacques Carvalho Ribeiro Filho [1], Eunice Maia de Andrade [2], Maria Simas Guerreiro [3,*], Helba Araújo de Queiroz Palácio [4] and José Bandeira Brasil [1]**

[1] Departamento de Engenharia Agrícola, Campus do Pici, Universidade Federal do Ceará, Fortaleza CEP 60455-760, Brazil
[2] Departamento de Conservação de Solo e Água, Universidade Federal Rural do Semi-Arido, Rua Francisco Mota, 572, Mossoró CEP 59625-900, Brazil
[3] I3ID, Universidade Fernando Pessoa, Praça 9 de Abril, 349, 4249-004 Porto, Portugal
[4] Instituto Federal de Educação, Ciência e Tecnologia do Ceará, Rodovia Iguatu-Várzea Alegre km, 5, Iguatu CEP 63503-790, Brazil
* Correspondence: mariajoao@ufp.edu.pt

**Abstract:** Soil's physical and hydrological properties influence the proper modeling, planning, and management of water resources and soil conservation. In areas of vertic soils subjected to wetting and drying cycles, the soil–water–atmosphere interaction is complex and understudied at the field scale, especially in dry tropical regions. This work quantifies and analyzes crack development under field conditions in an expansive soil in a semiarid region for both the dry and rainy seasons. Six 1 $m^2$ plots in an experimental 2.8 ha watershed were photographed and direct measurements were taken of the soil moisture and crack area, depth and volume once a week and after a rainfall event from July 2019 to June 2020. The rainfall was monitored for the entire period and showed a unimodal distribution from December to May after five months without precipitation. The cracks were first sealed in the plots with a predominance of sand and when the soil moisture was above 23% and had an accumulated precipitation of 102 mm. The other plots sealed their cracks when the soil moisture was above 32% and with an accumulated precipitation in the rainy season above 222 mm. The cracks redeveloped after sealing upon a reduction of 4% in the soil moisture. The depth of the cracks showed a better response to climatic variations (total precipitation, soil moisture and continuous dry and wet days). The higher clay content and the higher plasticity index plots developed more cracks with greater depth and volume.

**Keywords:** vertic soils; crack dynamics; tropical dry regions; semiarid



**Citation:** Ribeiro Filho, J.C.; Andrade, E.M.d.; Guerreiro, M.S.; Palácio, H.A.d.Q.; Brasil, J.B. Soil–Water–Atmosphere Effects on Soil Crack Characteristics under Field Conditions in a Semiarid Climate. *Hydrology* **2023**, *10*, 83. https://doi.org/10.3390/hydrology10040083

Academic Editors: Songhao Shang, Qianqian Zhang, Dongqin Yin, Hamza Gabriel and Magdy Mohssen

Received: 28 February 2023
Revised: 24 March 2023
Accepted: 2 April 2023
Published: 4 April 2023



## 1. Introduction

Arid and semiarid ecosystems account for approximately 29.8% of the Earth's surface [1]. Global warming and associated climate changes may increase the risk of extreme phenomena—droughts and heavy rains, which directly affect hydrological processes [1,2]. Forecasts of more extreme climate regimes will make arid and semiarid ecosystems become more vulnerable, with the possibility of increasing the total area of dry land globally [3].

Soil's physical, chemical and biological characteristics [1,4–7] influence runoff, infiltration and evapotranspiration [2,6,7], and some expansive clays (e.g., montmorillonite) swell and shrink during the wetting and drying processes [2,8], affecting the hydrologic processes.

Changes in the water content in expansive soils can significantly alter the hydromechanical behavior of a soil. These effects mainly include: (1) voluminous change due to swelling and shrinkage, and (2) variation in mechanical behavior, such as strength (or stress) and compression [8]. Soils and clay minerals absorb water and expand upon wetting, and they shrink and form desiccation cracks as they dry. Cracks modify the processes of infiltration, flow, evapotranspiration, and redistribution of water in the soil profile [4,6,9],

and they also form preferential flow channels with faster transport of water and nutrients (solutes) that negatively affect irrigation and soil fertilization for agricultural use [5,10].

The expansion/contraction characteristic of these soils has implications for distinct fields—in geotechnical engineering, where the formation of crack networks can destroy the integrity of the soil structure, damaging road structures and other civil construction infrastructures [7,11]; and in agriculture, where soil cracks may impose limitations on crop production [12], promote physical damage to plant roots, encourage the vertical movement and leaching of dissolved nutrients beyond the root zone, provide extra surface for moisture loss, and even promote rill erosion.

Drought-induced cracks in the soil are usually complex network structures. The accurate acquisition of cracks' morphometric data is not only a prerequisite for obtaining the relevant crack networks' geometric parameters, but also a basis for better understanding the cracks' development mechanism and defining procedures to promote or minimize soil cracks [13,14].

Research on cracks in expansive soils has been mostly conducted in controlled environments for the quantification of the geometry of a single crack and the morphology of crack networks [1,2,5,15,16], and not so much in field-scale studies to understand the dynamics of the cracks through in situ observations of the soil surface [2,8,16]. Changes in the hydraulic properties of expansive soils (e.g., soil moisture) under field conditions may help explain the response of soil cracks' properties to climate dynamics in time [2,5].

The objectives of this study were to (a) assess and quantify the soil characteristics and dynamics that govern the crack formation and healing processes under natural conditions; and (b) quantify the soil moisture limits on the response of soil swelling and shrinking in the wet and dry seasons in a vertic soil in a semiarid region under natural conditions.

## 2. Materials and Methods

### *2.1. Study Area*

The experimental area is a 2.8 ha first-order catchment with a 5.6% slope. The soil has a depth of 2.0 m and is classified as vertisol, with a predominance of expansive 2:1 clay minerals from the montmorillonite group [17]. It is located in a representative fragment of a seasonally dry tropical dry forest in northeastern Brazil (Figure 1) under vegetation regeneration after clearing, burning and planting pasture in 2010.

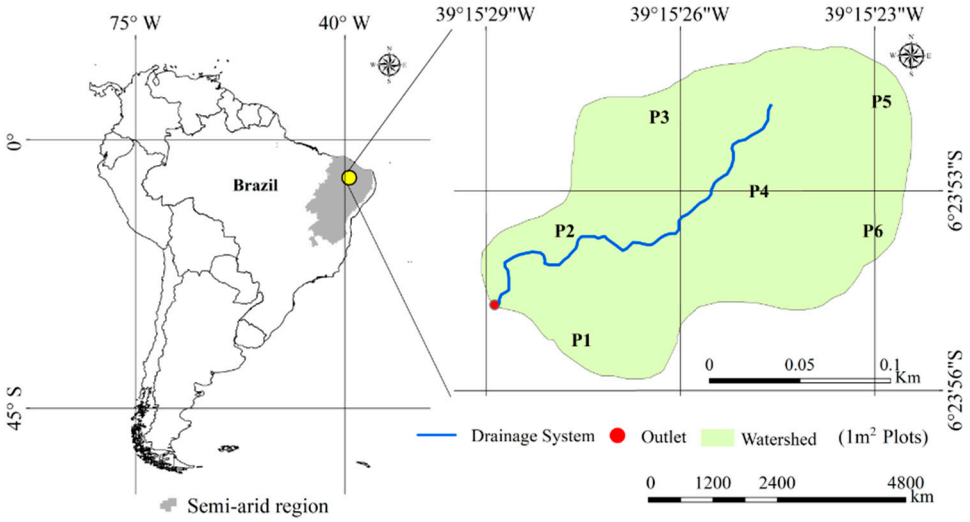


**Figure 1.** Study area location.

The climate is classified as a subtropical steppe (BSh—low-latitude semiarid or dry), according to Köppen's classification. With an aridity index of 0.48, it has a mean annual potential evapotranspiration of 2113 mm year$^{-1}$ and a mean annual precipitation of

997 ± 300 mm. Some 89% percent of the annual rainfall is concentrated in the wet semester of December to May (Figure 2) [18,19].

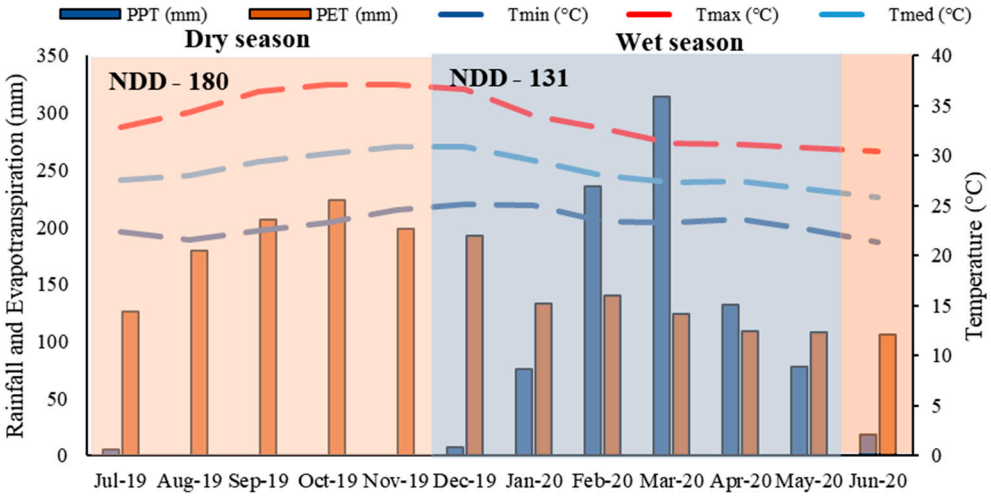


**Figure 2.** Mean rainfall; potential evapotranspiration; minimum, maximum and average temperatures; and average number of dry days for the wet and dry seasons in the study area from 1980 to 2020. PPT is the average monthly rainfall (mm); PET is the average monthly potential evapotranspiration (mm); Tmin, Tmax, and Tmed are the average monthly minimum, maximum, and mean temperatures (°C), respectively, for the study period; and NDD is the seasonal average number of dry days from 1980 to 2020.

Soil samples were collected with a sampling probe for textural classification and determination of the physical characteristics at each plot. A cluster analysis was performed on the soil characteristics to explore the naturally occurring groups using the software IBM SPSS Statistics 27.

### *2.2. Monitoring*

Rainfall was assessed using a Ville de Paris rain gauge. The soil moisture content was determined weekly and after a rainfall event by means of the gravimetric method in triplicate. Soil samples were collected outside the border of each plot, as this border sampling pattern better estimates the soil moisture of the plot without compromising its soil structure.

The soil cracks were monitored at six 1 $m^2$ (1 m × 1 m) randomly located experimental plots (Figure 1) for one year—1 July 2019 to 30 June 2020 (Figure 3). All the vegetation inside and around the plots was removed before the field measurements (at least weekly), keeping the plots free of vegetation for the entire period of study to minimize the soil structure changes.

The crack monitoring consisted of the in situ location of the cracks and the measurement of their respective depth. Cracks were identified with the aid of a 0.05 m × 0.05 m net placed over the 1 $m^2$ experimental plots, totaling a mesh of 400 points (Figure 4). The crack depth was measured using a 4 mm diameter rod and a ruler at the intersection of each crack and the 0.05 m × 0.05 m net (Figure 4).

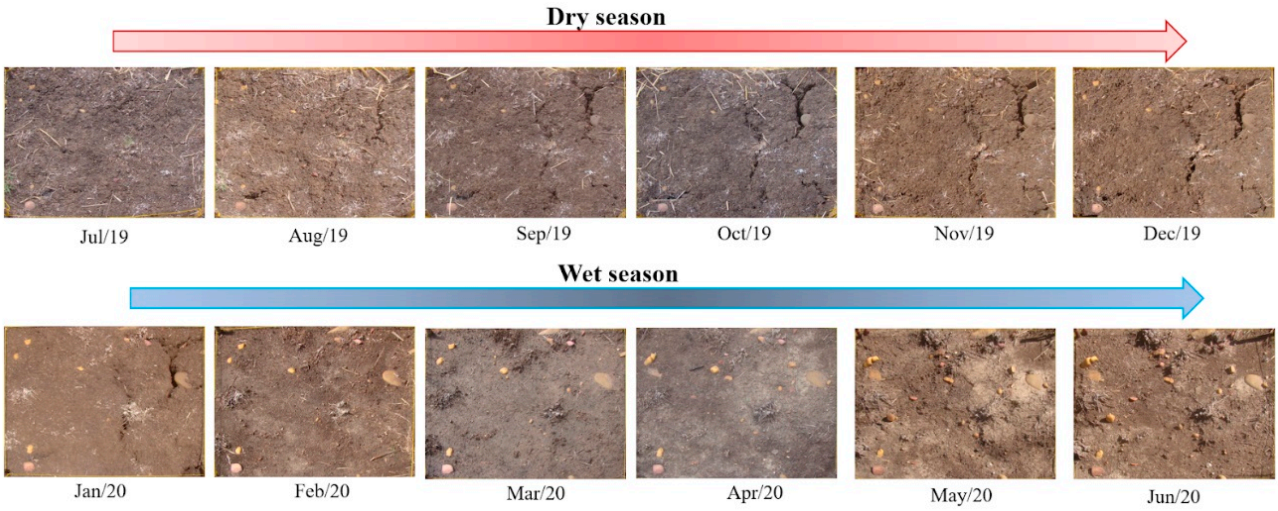


**Figure 3.** Monthly development of soil cracks in an experimental plot.

**Figure 4.** Crack monitoring in situ.

### *2.3. Crack Morphology and Dynamics*

The recognition of individual cracks and the assessment of the respective surface area, average width, and length was performed using the software Crack Image Analysis System Version 2.32 (CIAS) [20] based on the in situ acquired images (Figure 5). A Sony® DSC-H9 camera placed on a tripod always at the same location collected the plot images. Photogra hic images were taken at the best light hours (between 12:00 and 1:00 p.m.), except on rainy days, when photos were taken after the end of the event or on the next morning.

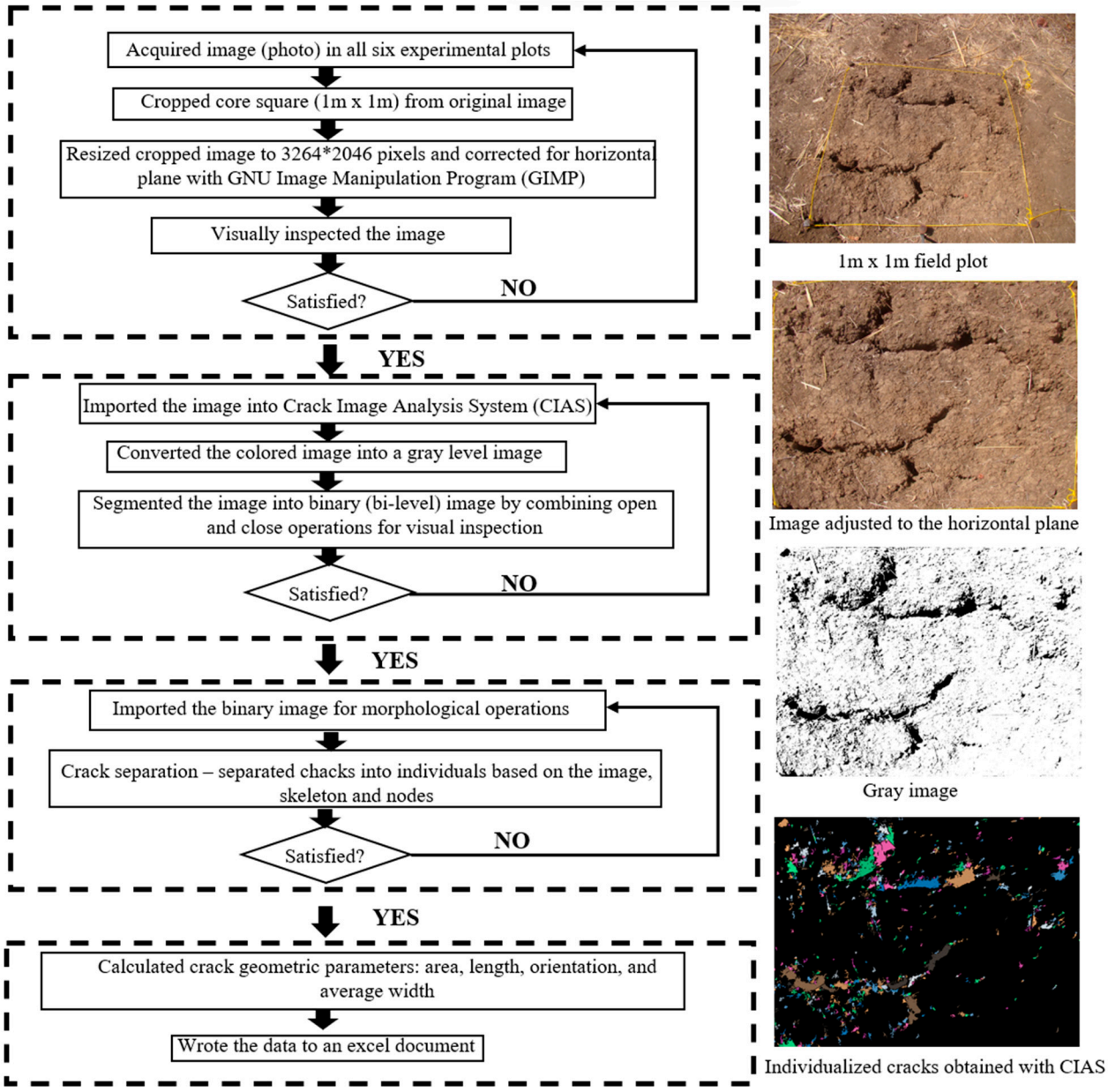


**Figure 5.** Methodology for image collection, correction and parameter calculation.

The volume of the cracks was computed using the crack average depth obtained via the in situ monitoring and the area was assessed using the CIAS software Version 2.32, as proposed by [21]. The soil crack area density (*Dc*) (Equation (1)) was evaluated using the method proposed also by [21]. The level of development (Table 1) was based on [16]:

$$Dc = \frac{a_c}{A_t} * 100 \quad (1)$$

where $a_c$ is the crack area ($m^2$) and $A_t$ is the total area (1 $m^2$).

The crack area velocity represents the rate of development of the crack area in both the swelling and the shrinking stages. The assessment of the temporal and spatial variability of the cracks' swelling and shrinking included the crack area formation velocity and associated correlations with climate factors, soil moisture and soil characteristics. We assumed the linear variation of the parameters (Dc, depth, and soil moisture) with time between field monitoring visits. All the analyses were based on the average depth, total area and total volume of the cracks at each plot.

**Table 1.** Soil cracks' level of development based on the crack area density.

| Dc Intervals | Levels of Development |
|---|---|
| Dc $\leq$ 5% | Feeble |
| 5 < Dc $\leq$ 10 | Light |
| 10 < Dc $\leq$ 22 | Medium |
| 22 < Dc $\leq$ 27 | Intensive |
| Dc > 27 | Extremely intensive |

## 3. Results

### *3.1. Field Data*

A total rainfall of 869 mm distributed in 54 events (Figure 6) was recorded during the study period (19 July–20 June). Only three rainfall events occurred in the dry season, with a total of 9 mm that led to no runoff. The wet season had seven runoff events in both February and March and one runoff event in May. February showed 23% of the rainfall of the wet season (12 events), and March concentrated 33% of that rainfall (17 events). The cracks were sealed for 16 days in March and opened after 2 consecutive days without precipitation.

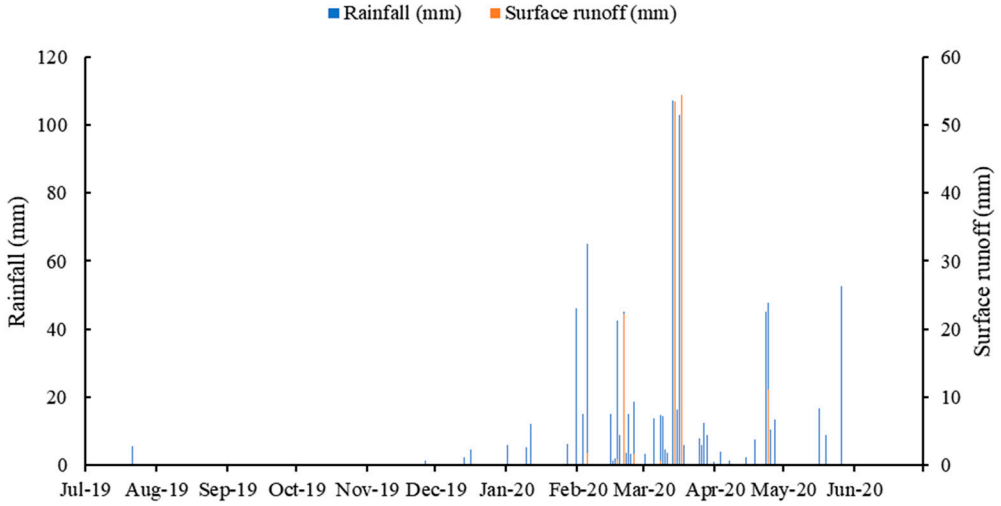


**Figure 6.** Rainfall and runoff events in the study period.

The total sealing of the cracks occurred on 18 February 2020, with an accumulated rainfall of 236 mm, of which 75% of the rainfall events were less than 10 mm and 52% less than 5 mm. During the first surface runoff event of the year (5 February 2020), the cracks were not totally sealed, although there were no surface cracks upon the occurrence of the other runoff events.

The spatial variability of the soils in the catchment was highlighted by the plots' physical soil properties (Table 2). Plots P3 and P6 stood out for the sand content (above 40%), classifying them as sandy clay loams—SCL (Table 2). The plasticity index (PI) and liquid limit (LL) in both plots showed the lowest values, as well as the base saturation (percentage of cation exchange capacity occupied by base cations) due to the sand content of these soils.

A cluster analysis of the soil properties of the experimental plots revealed two groups: one formed by the clay loam plots (CL) and the other formed by the sandy clay loam plots (SCL). This was confirmed by the significant difference ($p$-value < 0.05) in the physical parameters between the soils in plots P3 and P6 and the others (Figure 7). The P3 and P6 plots were more distant from the stream (Figure 1), suggesting that there was transport of finer particles to the lower zone (i.e., stream).

**Table 2.** Soil properties of the experimental plots.

| Soil Properties | Experimental Plots | | | | | |
|---|---|---|---|---|---|---|
| | **P1** | **P2** | **P3** | **P4** | **P5** | **P6** |
| Grain size analysis | | | | | | |
| Sand (%) | 21 | 26 | 41 | 22 | 27 | 44 |
| Silt (%) | 43 | 46 | 33 | 41 | 41 | 36 |
| Clay (%) | 36 | 28 | 26 | 37 | 32 | 20 |
| Organic matter (%) | 0.8 | 1.5 | 1.3 | 1.4 | 1.9 | 2.2 |
| Base saturation (%) | 92 | 95 | 84 | 95 | 92 | 89 |
| pH | 6.6 | 7.1 | 6 | 6.8 | 6.6 | 6.7 |
| Specific gravity | 2.79 | 2.57 | 2.53 | 2.53 | 2.48 | 2.52 |
| Liquid limit (%) | 43 | 38 | 28 | 42 | 40 | 33 |
| Plastic limit (%) | 14 | 27 | 21 | 32 | 26 | 27 |
| Plasticity index | 30 | 12 | 7 | 10 | 14 | 7 |
| Textural classification | Clay loam | Clay loam | Sandy clay loam | Clay loam | Clay loam | Sandy clay loam |

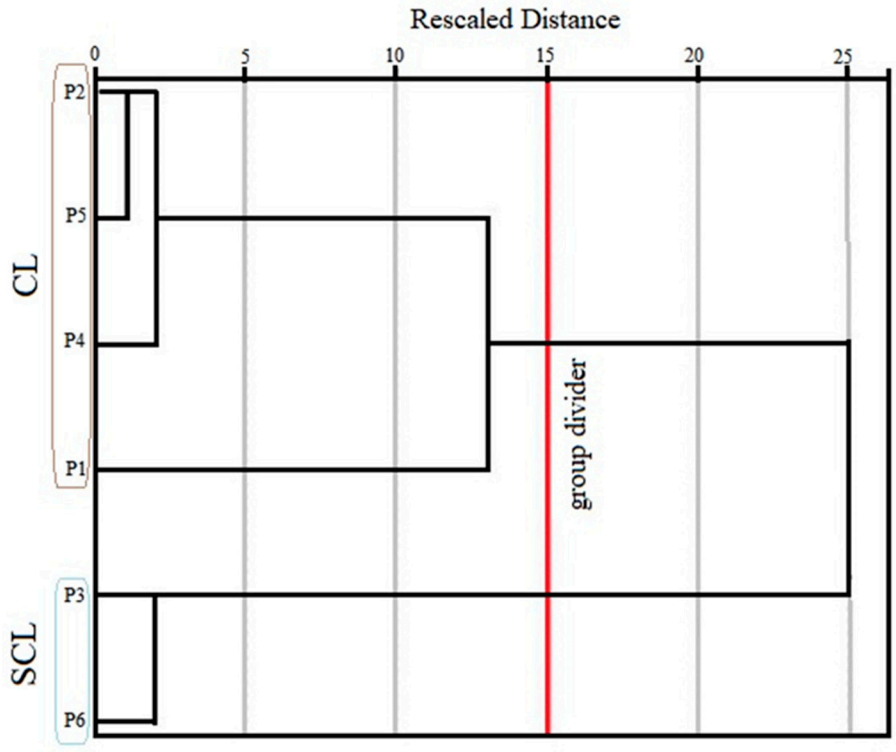


**Figure 7.** Cluster analysis results concerning the plots' soil characteristics. CL represents the clay loam cluster and SCL represents the sandy clay loam cluster.

### *3.2. Crack Morphology*

The crack depth in the clay loam plots varied from zero (no surface cracks) to a maximum depth of 0.12 m to 0.22 m (Figures 8 and 9). The maximum values were observed in P1, closer to the outlet, where the soil showed greater plasticity (Table 1).

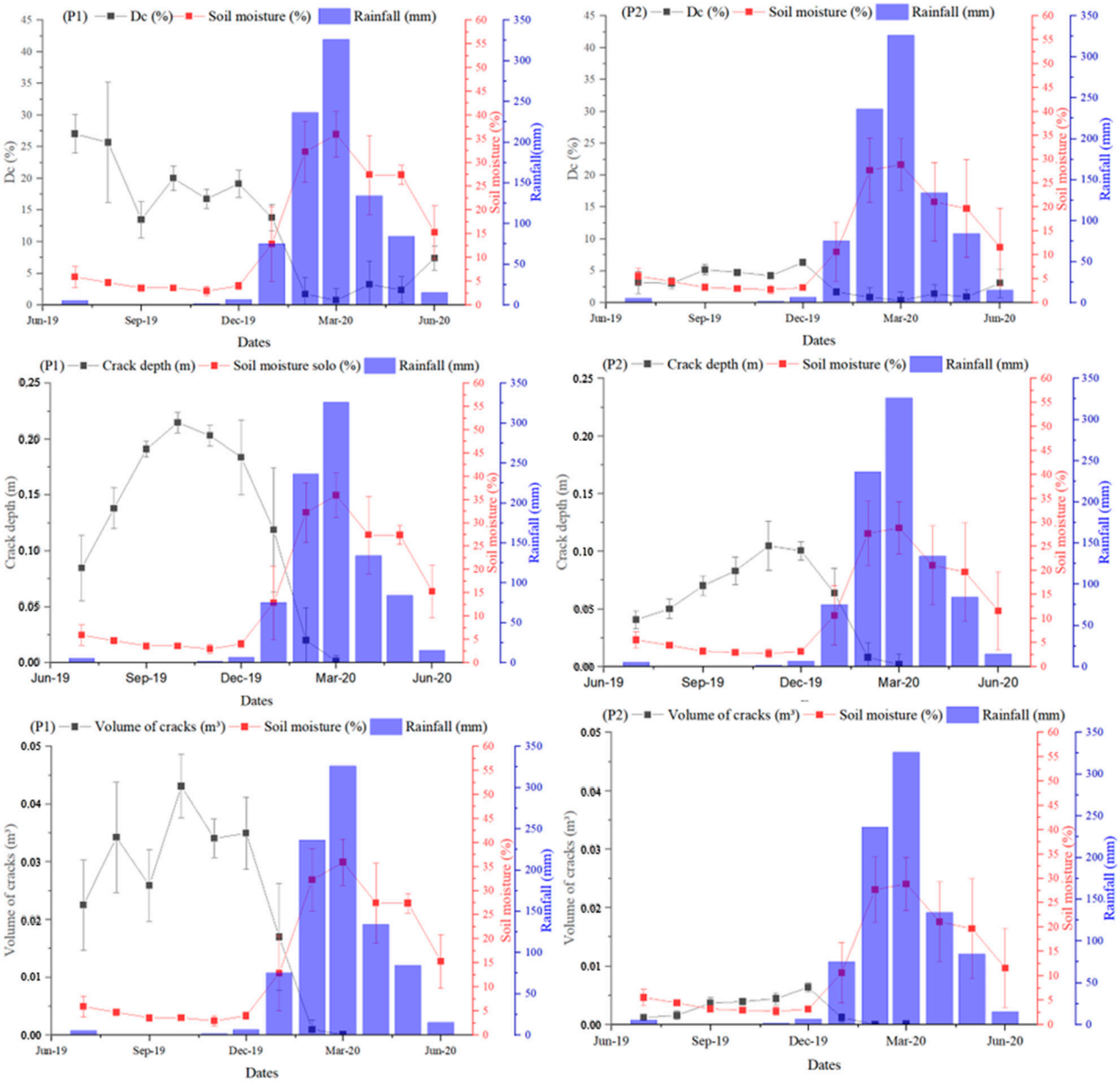


**Figure 8.** CL cluster plots P1 and P2—monthly Dc, area, depth, soil moisture and rainfall.

On the sandy clay loam plots, the cracks' depth varied from zero (no surface cracks) to 0.06 m (P3), as evidenced by Figure 10. The cracks showed an approximately constant value of 0.04 m after confirmation of the dry season in July–August and remained constant until the beginning of the rainy season in December. The plots with the least Dc and crack volume variability were the sandy clay loam plots—P3 and P6 (Figure 10), which also showed a lower fine particle percentage (<60%), a lower plasticity index (7.0), and a liquid limit below 33% (Table 2).

Based on the number of soil cracks and the respective morphometric characteristics, we observed a greater number, depth, and volume at the end of the dry season (Figures 8–10), as expected. The deepest cracks and higher Dc and crack volume were recorded in the CL group plots (P1—downstream and P5—upstream), as well as the greatest variability in these parameters. The smallest variability in the depth of the cracks, Dc and crack volume occurred in the sandy clay loam plots, with the lowest fine particle contents (P3 and P6). The lowest monthly mean values were recorded in the P6 plot—0.035 m and 0.0013 $m^3$ for the crack depth and crack volume, respectively (in the dry period).

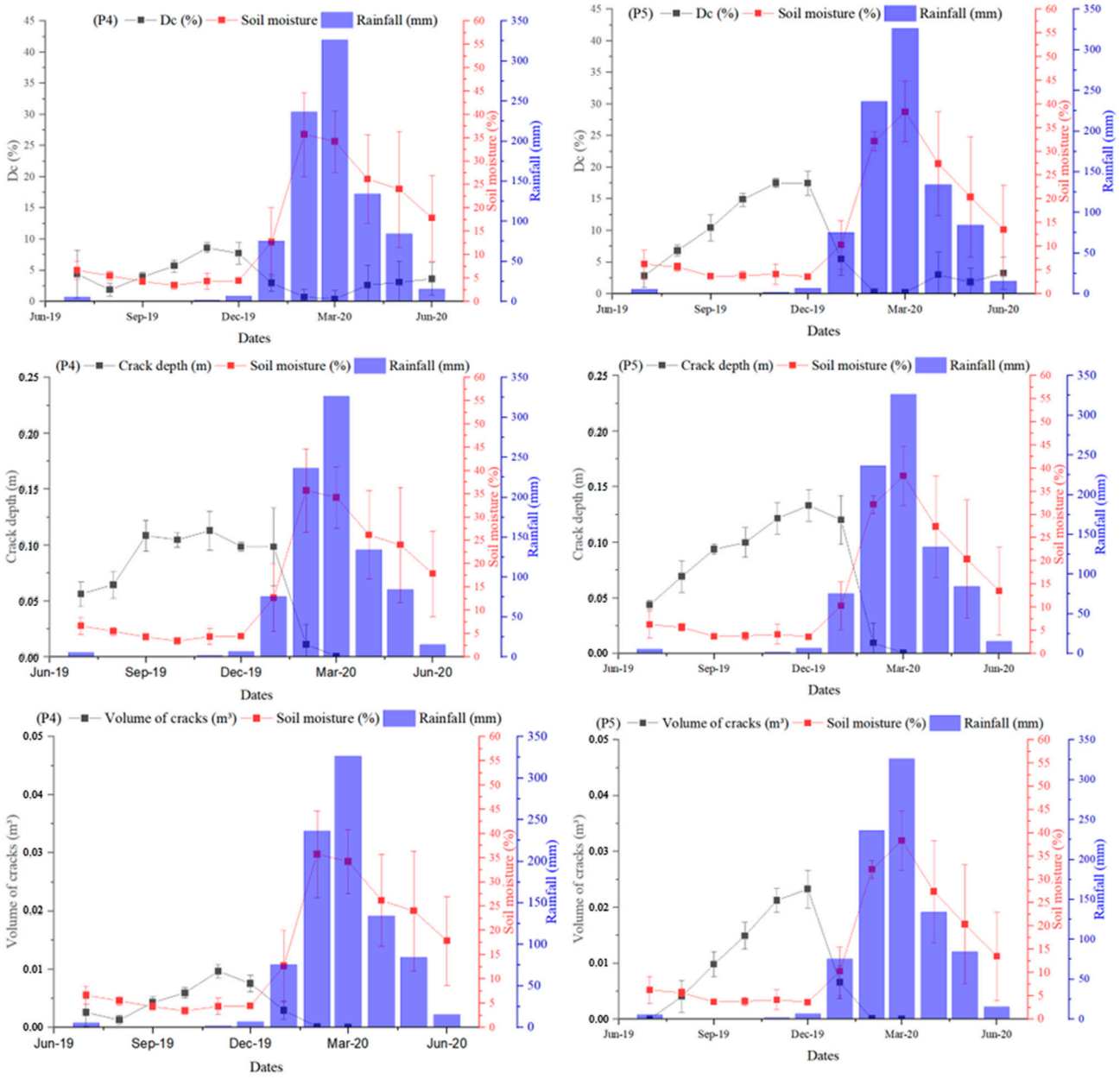


**Figure 9.** CL cluster plots P4 and P5—monthly Dc, area, depth, soil moisture and rainfall.

In the dry period, the crack depth varied from 0.034 m to 0.225 m (both in plot P1) in the clay loam plots (Figures 8 and 9), whereas in the sandy clay loam plots, the variation was smaller—0.026 m to 0.066 m (both in plot P6) (Figure 10). For a small variation in the soil moisture content, there was a quick response from the crack depth in the clay loam plots when compared to the sandy clay loam plots, which showed little response.

The rainfall accumulation until February was 87.1 mm, which was not enough to totally close the cracks—the crack depth was higher in the clay loam plots than in the sandy loam plots. Even though there was precipitation in the wet season after March, the wettest month of the year, the monthly rainfall decreased, with an increasing response from the Dc at all the plots (Figures 8–10).

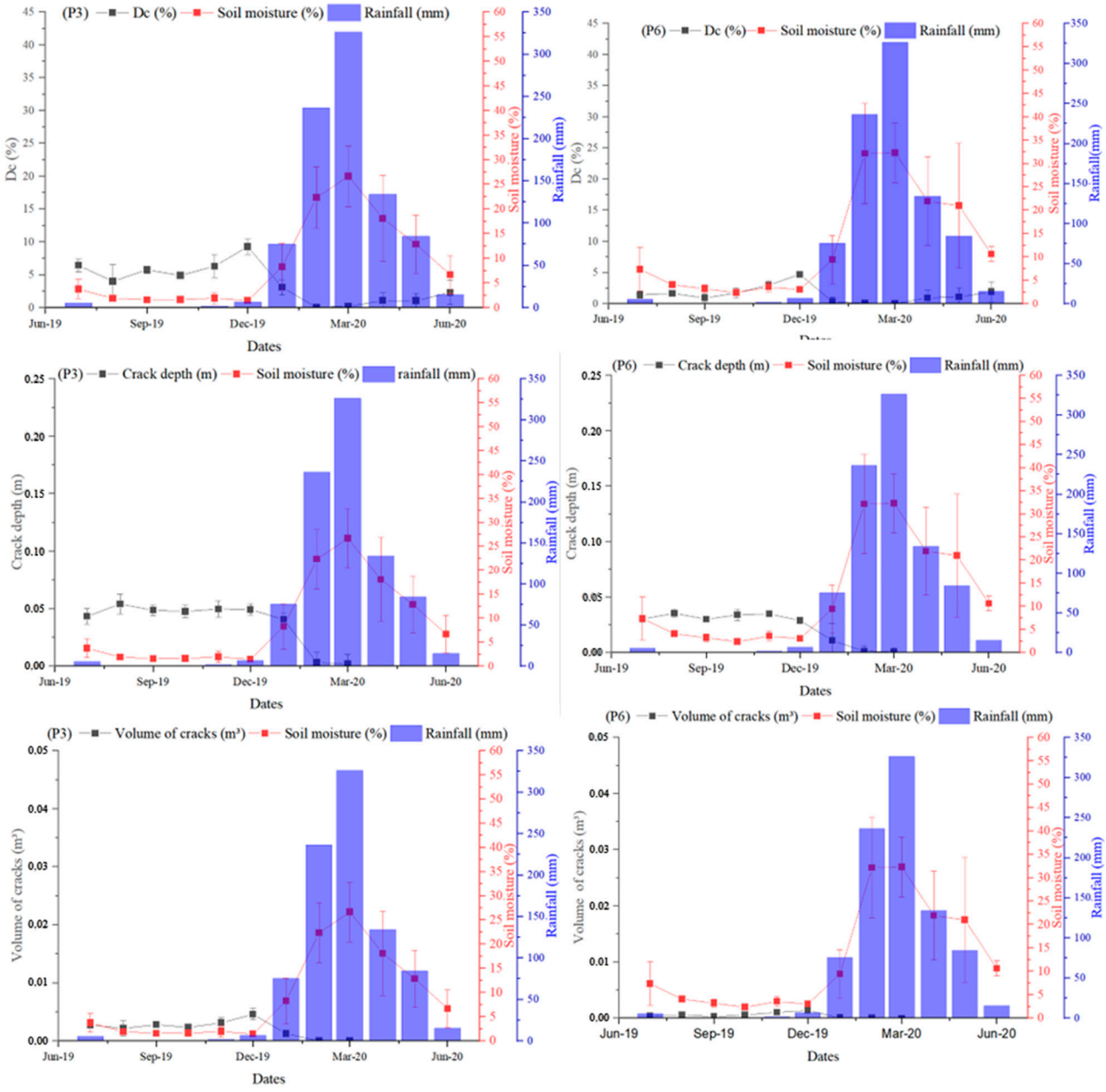


**Figure 10.** SCL cluster plots P3 and P6—monthly Dc, area, depth, soil moisture and rainfall.

### *3.3. Crack Dynamics*

The Dc showed a significant logarithmic correlation with the soil moisture content ($p < 0.001$) in all the plots of the CL group (Figure 11). The SCL group (Figure 12) did not show a significant correlation ($p < 0.001$) in either plot.

The SCL cluster plots showed an initial crack sealing process (Dc = 0) 70 days after the beginning of the rainy season, with a cumulative rainfall of 102 mm and a soil moisture content above 23% (Figures 10 and 12). As for the CL group (Figures 8 and 9), the sealing only occurred 87 days after the beginning of the rainy season, with a total cumulative rainfall of 222 mm, a soil moisture content above 32% (Figure 11), and after a rainfall event of 52.4 mm. There seemed to be no pattern in the response of the soil crack area to a soil moisture content of up to 7% in the SCL and 13% in the CL plots, respectively.

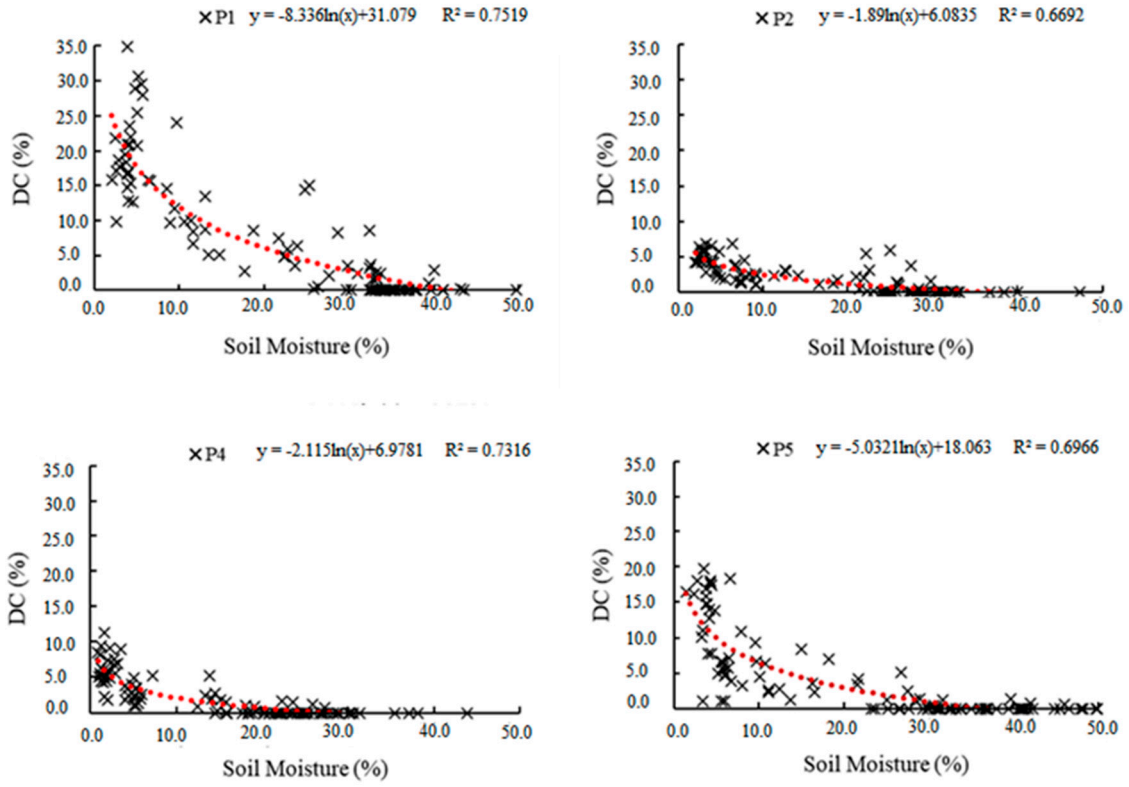


**Figure 11.** Soil moisture vs. Dc for the CL cluster plots P1, P2, P4 and P5.

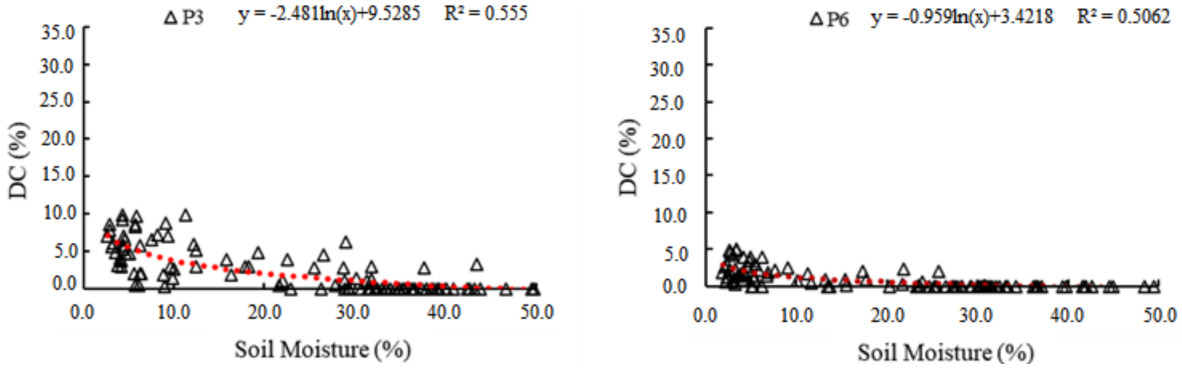


**Figure 12.** Soil moisture vs. Dc for the SCL cluster plots P3 and P6.

A closer look at the swelling and shrinking behavior of the soil highlighted a remarkable difference between the CL plots and the SCL plots—a maximum value of the soil crack area density of 0.37 $m^2$ in the CL plots against 0.10 $m^2$ in the SCL plots, and crack occurrence up to a soil moisture content of 43% in the CL against 27% in the SCL (Figure 13a,b).

The limit to the crack opening and sealing on the drying and wetting cycles showed a difference of 6% in the soil moisture content—when drying, the CL plots started opening cracks at a soil moisture below 43%, whereas as it reached a soil moisture content of 37% upon wetting, the cracks were sealed. Similar behavior was observed in the SCL plots, with a smaller difference of 3% in the soil moisture content, which began the crack opening process at a soil moisture content below 27% when drying and a soil moisture content below 24% when wetting (Figure 13c,d).

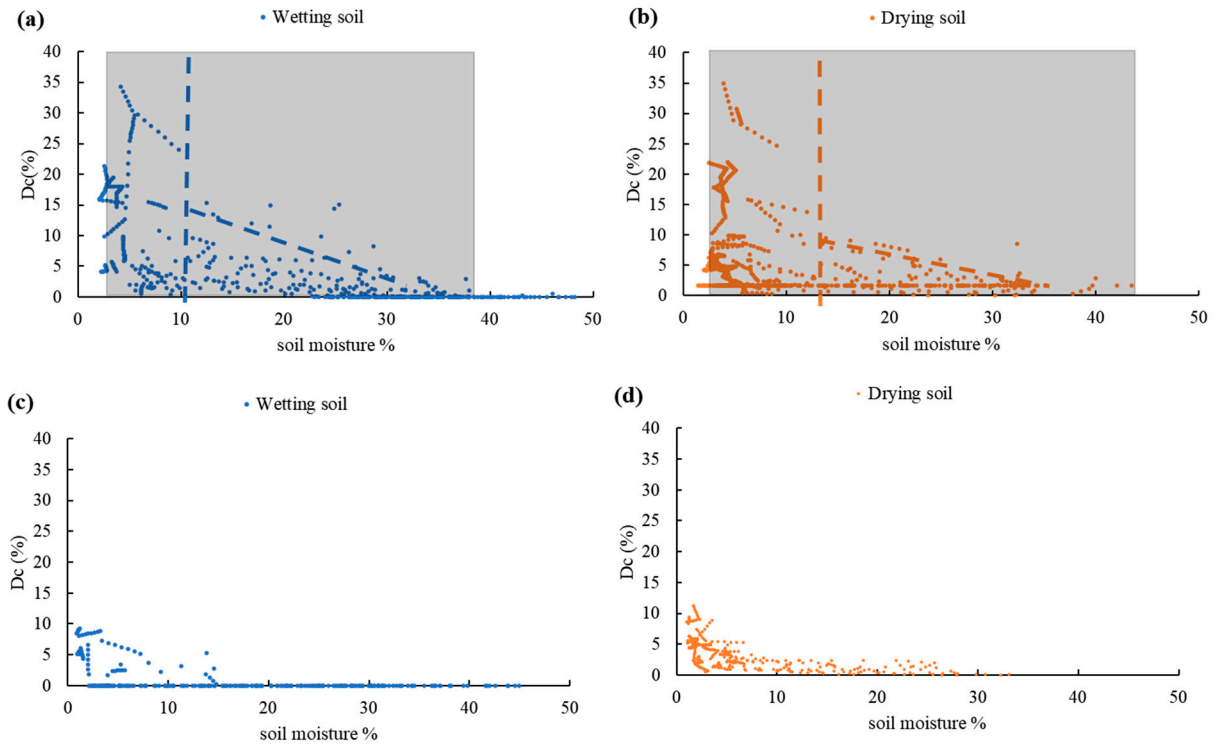


**Figure 13.** Crack area density: (**a**) for wetting soil—CL; (**b**) for drying soil—CL; (**c**) for wetting soil—SCL; and (**d**) for drying soil—SCL.

The crack area opening/closing response velocity (Figure 14) in the CL was below 0.1 $m^2$ $day^{-1}$ and in the SCL below 0.06 $m^2$ $day^{-1}$ (just above half the response velocity of the CL). The fastest response time of the crack opening/sealing to the soil moisture was below 45% in the CL and below 28% in the SCL. There was a remarkable difference in the crack response in the soils with finer particles above 70% (CL) relative to the soil moisture despite the clay content, both upon the drying and wetting cycles.

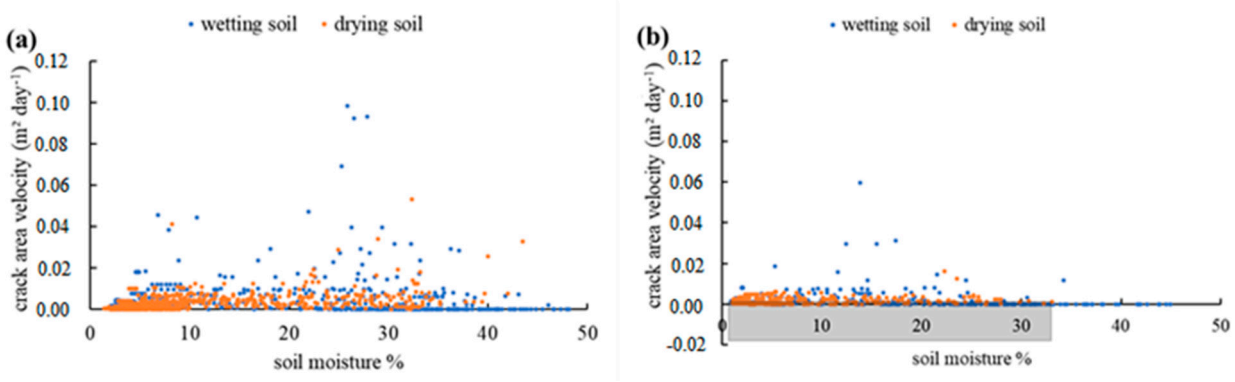


**Figure 14.** Velocity of crack opening/closure ($m^2$/day) in the (**a**) CL and (**b**) SCL plots.

## 4. Discussion

### *4.1. Crack Morphology*

The swelling and shrinking processes in expansive clay soils showed sensitivity to the fine particle content. The limits of the soil moisture content on the soil crack formation and sealing were significantly different for the clay loams and sandy clay loams, as were the crack area density limits [22].

The shrinking of expansive clays during dry periods and swelling with the occurrence of wet days [23] promote an increase/decrease in the depth, intensity, and volume of

cracks (Figures 6 and 8–10). After a rainfall event, both in the wet and dry seasons, the clay swelling process began in the surface layers as the hydrostatic forces increased [2], promoting the sealing of micro cracks even before the surface runoff process began. At the onset of the surface runoff, the cracks were not all sealed (Figures 6 and 8–10), and the deeper cracks acted as preferential flow paths [4,15], which influenced solute transport—the faster water and dissolved solutes flowed through the preferential paths with reduced soil sorption opportunities by the clay particles, promoting considerable water loss and groundwater pollution, as suggested by [24].

The smaller pores in the soils with higher clay contents promoted the development of high soil suction pressure [25] and cohesion [26], which led to crack formation. Water sorption by the clay particles at the deepest parts of the cracks promoted their closure in an upward movement and the reduction of the depth of the cracks throughout the rainy season (Figures 8–10).

The clay content in itself did not explain the different behavior of the crack area formation as a function of the soil moisture in this study—all the plots had a montmorillonite clay content above 30%. However, the behavior of the Dc as a function of the soil moisture (Figures 11 and 12) was different for both the sandy loam and the clay plots, which differed due to the fine particles content, liquid limit and plasticity. Such evidence resulted in the different volume of cracks between plot P1, with a higher volume and greater plasticity, and P4 and P5 (Figures 8–10), with lower volumes and lower plasticity indexes, although these plots, P1, P4 and P5, presented similar texture [2].

The process of crack sealing occurred gradually and inversely to the soil moisture content (Figures 8–10). From the beginning of the rainy season and until the total closure of the cracks, they generated preferential flow paths [4], depending mostly on the cumulative rainfall and depth of the event.

The expansion/contraction of the cracks in the soil was more sensitive in the wetting than in the drying process (Figure 13a,b). The SCL plots showed little response to crack formation for soil moisture contents between 5% and 25%, and no defined pattern relative to soil moisture contents below 5%. The CL plots showed a higher crack formation/sealing sensitivity for soil moisture contents between 13% and 42%, and no defined pattern relative to soil moisture contents below 13%. The expansion/shrinkage processes may respond differently to different climatic conditions due to the intrinsic soil characteristics, such as the granulometry and plasticity [2,27,28].

### *4.2. Crack Dynamics*

The reduction of 4% in the soil moisture (Figures 8–10) was enough for the emergence of cracks. As cracks formed, soil water evaporated in two dimensions—vertically via the soil surface and horizontally through the walls of the cracks [2], provided there was available water. As the water availability decreased, the velocity of the crack formation remained constant for both the clay loams and sandy clay loams, although it was faster in the clay loam plots (Figure 14). The swelling and shrinking processes occurred at a faster pace in the clay loam plots [1,26], as stressed by the different soil sealing time (Figures 8–10), suggesting correlation with their higher plasticity index (Table 1).

The degree of development of the cracks in the CL plots recorded a medium level of development for the Dc (Table 1), evidencing that the reduction of moisture in soils with higher rates of plasticity resulted in initially mild and then pronounced deformations when compared with the less plastic soils (SCL) [2,8]. The lower fine particle content in plots P3 and P6 (Table 2) reduced the degree of self-healing, as governed by the soil plasticity, which determines the potential for soil expansion and contraction [26].

It is known that the Dc decreases with the addition of water to the soil. During the dry season in this region, the possible sources of water entry into the soil are the processes of capillary rise and/or condensation of water vapor during the early morning hours [29]. The process of capillary rise was discarded, since there was no reduction in the depth of the cracks (Figures 8–10), evidencing a surface phenomenon.

Although there were no records of isolated precipitation events during the dry season (July to December) (except for three events > 10 mm, Figure 6), in August and September there was a reduction in the value of the Dc (Figures 8–10). The increase in the soil surface moisture content was believed to be the result of dew formation in other semiarid regions [1,30,31]. The process of increasing the soil moisture via the condensation process in the months with the lowest minimum temperatures is supported by [29] in an area adjacent to the studied watershed, raising the soil moisture at night by as much as 5%, which may be responsible for the reduction of the Dc (Figures 8–10).

The CL group presented an extremely intensive level of development (Figures 8 and 9), suggesting a need for greater initial abstractions to seal the surface cracks (Figures 6 and 8–10). There seemed to be a greater risk of soil and aquifer contamination during the drying process as the total crack area and depth were greater, offering preferential flow paths and a reduced opportunity for the adsorption of fertilizers by plants [24].

The sealing and formation of cracks in the SCL plots occurred at soil moisture contents above 25% and 27% in the wetting and drying processes, respectively. In the CL plots, these values were 38% and 43%, respectively. These results highlighted the hysteresis of these processes in both soil types, which may have occurred due to the fact that there was no increase in the soil moisture in the drying process and an increase and decrease in the soil moisture in the wetting processes. The soil moisture losses were mainly due to evaporation that occurred in two dimensions: horizontally via the soil surface and vertically from the walls of the cracks [4] and the rainfall events (Figure 6).

## 5. Conclusions

The intensity of the occurrence, maximum depth and volume of cracks vary according to the texture, limits of plasticity and soil liquidity. A lower fine particle content reduces the cracks' healing process, which is governed mostly by the soil plasticity. Higher fine particle contents lead to larger occurrence, depth and volume despite the clay content if associated with greater plasticity.

Cracks form after two consecutive dry days even during the wet season. The expansion/contraction of cracks in the soil is more sensitive in the wetting than in the drying process. Clay loams and sandy clay loams show different limits on the soil moisture content to start the opening and the sealing processes of crack formation.

There is no pattern in the response of crack formation to soil moisture contents below 5% and 13% for sandy clay loams and clay loams, respectively. The process of capillary rise impact on crack healing may be discarded, evidencing it being a surface phenomenon. There is a greater risk of soil and aquifer contamination during the drying process.

**Author Contributions:** All the authors made a significant contribution to the final version of the manuscript. Conceptualization, J.C.R.F., M.S.G., E.M.d.A. and H.A.d.Q.P.; methodology, M.S.G., J.B.B. and J.C.R.F.; writing—original draft preparation, J.C.R.F., M.S.G. and E.M.d.A.; writing—review and editing, all authors; supervision, M.S.G. and E.M.d.A.; project administration, E.M.d.A. All authors have read and agreed to the published version of the manuscript.

**Funding:** This work was supported by CNPq—Conselho Nacional de Desenvolvimento Científico e Tecnológico, Brazil (grant number 558135/2009-9).

**Data Availability Statement:** Data sharing is not applicable to this article.

**Acknowledgments:** This study was carried out with the support of the Coordenação de Aperfeiçoamento de Pessoal de Nível Superior—Brasil (CAPES), the Conselho Nacional de Desenvolvimento Científico e Tecnológico (CNPq) and the Fundação Cearense de Apoio ao Desenvolvimento Científico e Tecnológico (FUNCAP).

**Conflicts of Interest:** The authors declare that they have no conflict of interest.

## References


1. Wang, C.; Zhang, Z.Y.; Qi, W.; Fan, S.M. Morphological approach to quantifying soil cracks: Application to dynamic crack patterns during wetting-drying cycles. *Soil Sci. Soc. Am. J.* **2018**, *82*, 757–771. [CrossRef]
2. Tang, C.S.; Zhu, C.; Cheng, Q.; Zeng, H.; Xu, J.J.; Tian, B.G.; Shi, B. Desiccation cracking of soils: A review of investigation approaches, underlying mechanisms, and influencing factors. *Earth-Sci. Rev.* **2021**, *216*, 103586. [CrossRef]
3. Dai, A. Increasing drought under global warming in observations and models. *Nat. Clim. Chang.* **2013**, *3*, 52–58. [CrossRef]
4. Santos, J.C.N.; de Andrade, E.M.; Guerreiro, M.J.S.; Medeiros, P.H.A.; de Queiroz Palácio, H.A.; de Araújo Neto, J.R. Effect of dry spells and soil cracking on runoff generation in a semiarid micro watershed under land use change. *J. Hydrol.* **2016**, *541*, 1057–1066. [CrossRef]
5. Bordoloi, S.; Ni, J.; Ng, C.W.W. Soil desiccation cracking and its characterization in vegetated soil: A perspective review. *Sci. Total Environ.* **2020**, *729*, 138760. [CrossRef]
6. Sadeghi, S.H.; Kheirfam, H.; Darki, B.Z. Controlling runoff generation and soil loss from field experimental plots through inoculating cyanobacteria. *J. Hydrol.* **2020**, *585*, 124814. [CrossRef]
7. Cheng, Q.; Tang, C.S.; Xu, D.; Zeng, H.; Shi, B. Water infiltration in a cracked soil considering effect of drying-wetting cycles. *J. Hydrol.* **2021**, *593*, 125640. [CrossRef]
8. Tang, C.S.; Wang, D.Y.; Zhu, C.; Zhou, Q.Y.; Xu, S.K.; Shi, B. Characterizing drying-induced clayey soil desiccation cracking process using electrical resistivity method. *Appl. Clay Sci.* **2018**, *152*, 101–112. [CrossRef]
9. Tang, C.S.; Shi, B.; Liu, C.; Suo, W.B.; Gao, L. Experimental characterization of shrinkage and desiccation cracking in thin clay layer. *Appl. Clay Sci.* **2011**, *52*, 69–77. [CrossRef]
10. Ralaizafisoloarivony, N.; Degré, A.; Mercatoris, B.; Leonard, A.; Toye, D.; Charlier, R. Assessing Soil Crack Dynamics and Water Evaporation during Dryings of Agricultural Soil from Reduced Tillage and Conventional Tillage Fields. *Multidiscip. Digit. Publ. Inst. Proc.* **2020**, *30*, 59. [CrossRef]
11. Al-Jeznawi, D.; Sanchez, M.; Al-Taie, A.J. Using image analysis technique to study the effect of boundary and environment conditions on soil cracking mechanism. *Geotech. Geol. Eng.* **2021**, *39*, 25–36. [CrossRef]
12. Elias, E.A.; Salih, A.A.; Alaily, F. Cracking patterns in the Vertisols of the Sudan Gezira at the end of dry season. *Int. Agrophysics* **2021**, *15*, 151–155.
13. Wei, X.; Hattab, M.; Bompard, P.; Fleureau, J.M. Highlighting some mechanisms of crack formation and propagation in clays on drying path. *Géotechnique* **2016**, *66*, 287–300. [CrossRef]
14. Xu, J.J.; Zhang, H.; Tang, C.S.; Cheng, Q.; Liu, B.; Shi, B. Automatic soil desiccation crack recognition using deep learning. *Géotechnique* **2022**, *72*, 337–349. [CrossRef]
15. Dinka, T.M.; Morgan, C.L.; McInnes, K.J.; Kishné, A.S.; Harmel, R.D. Shrink–swell behavior of soil across a Vertisol catena. *J. Hydrol.* **2013**, *476*, 352–359. [CrossRef]
16. Xiong, D.; Yan, D.; Long, Y.; Lu, X.; Han, J.; Han, X.; Shi, L. Simulation of morphological development of soil cracks in Yuanmou Dry-hot Valley region, Southwest China. *Chin. Geogr. Sci.* **2010**, *20*, 112–122. [CrossRef]
17. Natural Resources Conservation Service. *Keys to Soil Taxonomy*, 12th ed.; Government Printing Office: Washington, DC, USA, 2014.
18. Campos, D.A.; de Andrade, E.M. Seasonal trend of climate variables in an area of the Caatinga phytogeographic domain. *Rev. Agro@mbiente On-Line* **2021**, *15*, 1–18. [CrossRef]
19. Guerreiro, M.S.; Maia de Andrade, E.; Palácio, H.A.D.Q.; Brasil, J.B.; Filho, J.C.R. Enhancing Ecosystem Services to Minimize Impact of Climate Variability in a Dry Tropical Forest with Vertisols. *Hydrology* **2021**, *8*, 46. [CrossRef]
20. Liu, C.; Tang, C.S.; Shi, B.; Suo, W.B. Automatic quantification of crack patterns by image processing. *Comput. Geosci.* **2013**, *57*, 77–80. [CrossRef]
21. Stewart, R.D.; Najm, M.R.A. Field measurements of soil cracks. *Soil Sci. Soci. Am. J.* **2020**, *84*, 1462–1476. [CrossRef]
22. Miller, W.L.; Kishné, A.S.; Morgan, C.L. Vertisol morphology, classification, and seasonal cracking patterns in the Texas Gulf coast prairie. *Soil Surv. Horiz.* **2010**, *51*, 10–16. [CrossRef]
23. Bullard, J.E.; Ockelford, A.; Strong, C.L.; Aubault, H. Impact of multi-day rainfall events on surface roughness and physical crusting of very fine soils. *Geoderma* **2018**, *313*, 181–192. [CrossRef]
24. Li, M.; Yao, J.; Yan, R.; Cheng, J. Effects of infiltration amounts on preferential flow characteristics and solute transport in the protection forest soil of southwestern China. *Water* **2021**, *13*, 1301. [CrossRef]
25. Ferreira, S.R.D.M.; Araújo, A.G.D.D.; Barbosa, F.A.S.; Silva, T.C.R.; Bezerra, I.M.D.L. Analysis of changes in volume and propagation of cracks in expansive soil due to changes in water content. *Revista Brasileira de Ciência do Solo* **2020**, *44*, 1–19. [CrossRef]
26. Rayhani, M.H.T.; Yanful, E.K.; Fakher, A. Physical modeling of desiccation cracking in plastic soils. *Eng. Geol.* **2008**, *97*, 25–31. [CrossRef]
27. Ribeiro Filho, J.C.; de Andrade, E.M.; Guerreiro, M.S.; de Queiroz Palácio, H.A.; Brasil, J.B. Climate Data to Predict Geometry of Cracks in Expansive Soils in a Tropical Semiarid Region. *Sustainability* **2022**, *14*, 675. [CrossRef]
28. Ribeiro Filho, J.C.; de Andrade, E.M.; de Sousa, M.M.M.; Brasil, J.B.; de Quairoz Palácio, H.A. Morphological characteristics of cracks in soil with and without vegetation cover. *Rev. Agro@mbiente On-Line* **2023**, *17*, 1–15. [CrossRef]
29. Guerreiro, M.S.; de Andrade, E.M.; de Sousa, M.M.M.; Brasil, J.B.; Filho, J.C.R.; de Queiroz Palácio, H.A. Contribution of non-rainfall water input to surface soil moisture in a tropical dry forest. *Hydrology* **2022**, *9*, 102. [CrossRef]

30. Dou, Y.; Quan, J.; Jia, X.; Wang, Q.; Liu, Y. Near-Surface Warming Reduces Dew Frequency in China. *Geophys. Res. Lett.* **2021**, *48*, e2020GL091923. [CrossRef]
31. Yu, B.; Liu, G.; Liu, Q.; Wang, X.; Feng, J.; Huang, C. Soil moisture variations at different topographic domains and land use types in the semi-arid Loess Plateau, China. *Catena* **2018**, *165*, 125–132. [CrossRef]